ESI material for

The emergence of intense near-infrared photoluminescence by photoactivation of silver nanoclusters

Wataru Ishii,[a] Shohei Katao,[a] Yoshiko Nishikawa,[a] Yasuo Okajima,[a] Atsuya Hatori,[b] Masahiro Ehara,[b] Tsuyoshi Kawai[a] and Takuya Nakashima[a]*

[a]Division of Materials Science, Graduate School of Science and Technology, Nara Institute of Science and Technology (NAIST), Ikoma, Nara 630-01921, Japan.

[b]Institute for Molecular Science, Research Center for Computational Science, Myodaiji, Okazaki 444-8585, Japan.

Experimental

Synthesis of $Ag_{29}(BDT)_{12}(TPP)_4$ NCs

$Ag_{29}(BDT)_{12}(TPP)_4$ NCs were prepared according to a method reported in the literature except that dichloromethane was used as a solvent in place of chloroform.[S1] Briefly, in a 50 mL glass vial, 36 μl of BDT was added to 28 mL of chloroform. To this solution, 13.3 mL of $AgNO_3$ solution in methanol (24 mM) was injected followed by the addition of TPP solution in chloroform (560 mg in 2.4 mL). The resulting mixture was allowed to stir for 15 min before the addition of an aqueous solution of $NaBH_4$ (28 mg in 1.4 mL). The mixture was stirred overnight (ca. 12h) to give orange precipitate. The precipitated NCs from the chloroform reaction solution were washed with ethanol followed by the redispersion in pyridine.

Synthesis of $Ag_{29-x}Au_x(BDT)_{12}(TPP)_4$ NCs

Au-doped Au_xAg_{29-x} NCs were also prepared according to the literature with the Au precursor concentration of 40 mol% Au.[S2] A similar procedure for the synthesis of $Ag_{29}(BDT)_{12}(TPP)_4$ NCs was applied. In place of 13.3 mL of $AgNO_3$ (24 mM) solution in methanol, 8 mL of $AgNO_3$ (24 mM) in methanol and 2.6 mL of chloro(triphenylphosphine) gold (I) (47 mM) in chloroform were used.

Photoactivation of NIR PL property

The pyridine solution of Ag_{29}-based NCs was irradiated by a Xenon short arc lamp (500 W) through a band pass filter (λ = 450 nm, FWHM = 10 nm). The intensity of incident light was measured to be 270 μWcm^{-2} at 450 nm. Although the excitation light at 450 nm in the steady-state PL and PLQY measurements with the measurement time less than 2 min gave the negligible effect on the PL property of NCs, the effect of laser irradiation (400 nm) for the PL lifetime measurement (> 5 min) could not be ignored.

Characterizations

ESI-MS spectrometry was conducted with a JEOL JMS-T100LP AccuTOF LC-plus 4G. UV-vis absorption spectra were recorded with a JASCO V-670 spectrophotometer. PL spectra were measured by a JASCO FP8500 and a Jobin Yvon SPEX Fluorolog-3 in degassed condition. A photomultiplier (Hamamatsu R5509-72) cooled at 193 K was used to detect NIR PL (Fluorolog-3). All the PL spectra were electronically corrected for instrumental response in FP8500 and Fluorolog-3 in the range of λ_{PL} < 850 nm and λ_{PL} > 650 nm, respectively. For the temperature-dependent PL study, the temperature of samples was controlled by an Oxford Instruments variable-temperature liquid nitrogen cryostat OptistatDN in the range from 80 K to room temperature. Absolute PLQY values were determined using a Hamamatsu C9920-02 (λ_{PL} < 950 nm) in pyridine-d_5. Emission lifetime was studied using a picosecond fluorescence measurement

system (Hamamatsu C4780) with a streak scope (Hamamatsu C4334). The excitation source was generated by a Nd:YVO_4 laser (Coherent, Verdi) pumped Ti:Sapphire laser system (Coherent, Mira-900) equipped with a cavity dumper (Coherent, PulseSwitch). This delivers 100 fs pulse trains at 800 nm. After the frequency was doubled with a LiB_3O_5 (LBO) crystal, the incident pulses were focused on the sample (λ_{ex} = 400 nm). PL spectrum of a single-crystal was measured with an Olympus BX-51 polarizing microscope connected to a Hamamatsu PMA-11 photodetector (> 800 nm) through an optical fiber. Excitation to the crystal was performed with a high-pressure mercury lamp through a band path filer (330–385 nm) and the emission was collected through a long path filter (> 420 nm). X-ray single crystal diffraction data were collected using a Rigaku VariMax with RAPID (1.2 kW) imaging plate area detector with connfocal mirror optics Mo Ka radiation at 103 K. All calculations were performed with the Rigaku Olex2 ver. 1.3.0 software.[S3] The structure was with the SHELXT[S4] structure solution program using Intrinsic Phasing and refined with SHELXL[S5] refinement package using Least Squares minimization. Some non-hydrogen atoms were refined anisotropically, while the rest were refined isotropically. The structure has significant alerts due to the disordering on the pyridine units. The disordered solvents in the crystal structure were flattened using 'Solvent Mask' option. The crystal data has been deposited to the Cambridge Structural Database and the CCDC number: 2076349

DFT calculations

The preliminary DFT and TDDFT calculations were conducted for the model Ag_{29} $(BDT)_{12}$ using B3LYP functional.[S6] The defect was modeled with $Ag_{29}(BDT)_{11}(BDT\text{-}Na^+)$ pyridine (pyr) (Fig. S). Relativistic effective core potential LANL2DZ [S7] was used for silver atoms and the basis sets of other atoms were 3-21G.[S8] For simulating absorption spectra, 300 excited states were solved to cover the spectrum in the energy range up to about 300 nm. The emission energies were obtained by optimizing S_1 state using TD-DFT calculation and T_1 state using DFT calculation. All calculations were conducted using Gaussian16 suite of programs version A.03.[S9] Calculated absorption spectrum with the Gaussian convolution (FWHM of 0.15 eV) is shown in Fig. S18 and the calculated emission energies are summarized in Table S1.

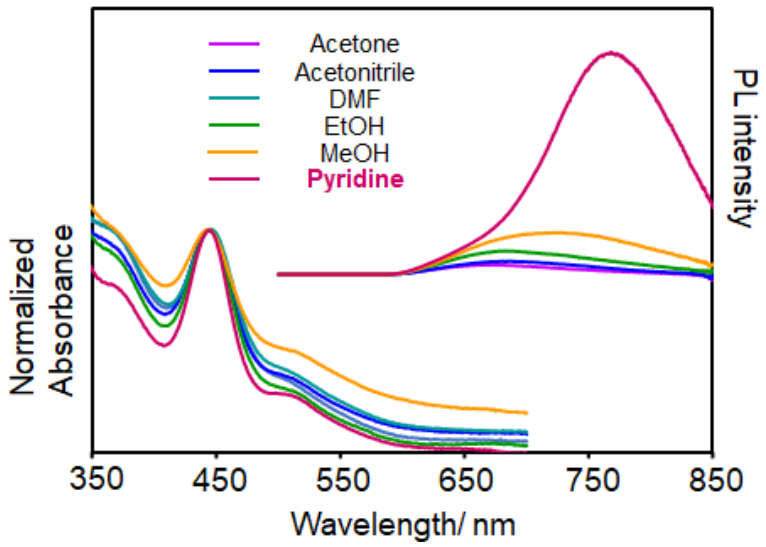

Fig. S1 Absorption and PL spectra of $Ag_{29}(BDT)_{12}(TPP)_4$ NCs in various solvents.

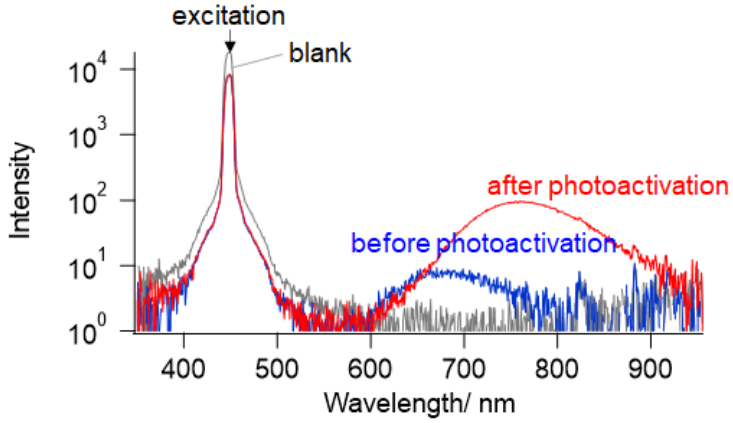

Fig. S2 Determination of absolute PLQY of Ag_{29} NCs before and after photoirradiation in pyridine-d_5.

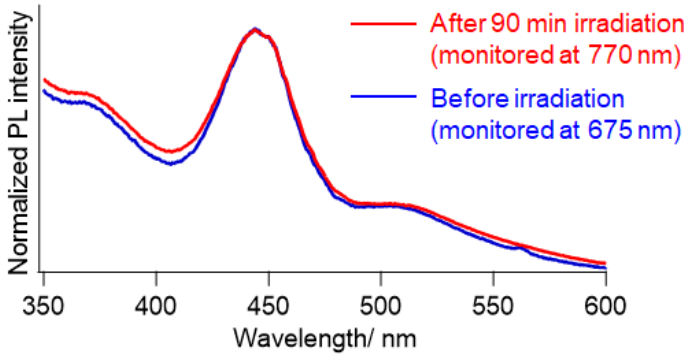

Fig. S3 Excitation spectra of $Ag_{29}(BDT)_{12}(TPP)_4$ NCs in pyridine before and after the photoirradiation monitored at 675 and 770 nm, respectively.

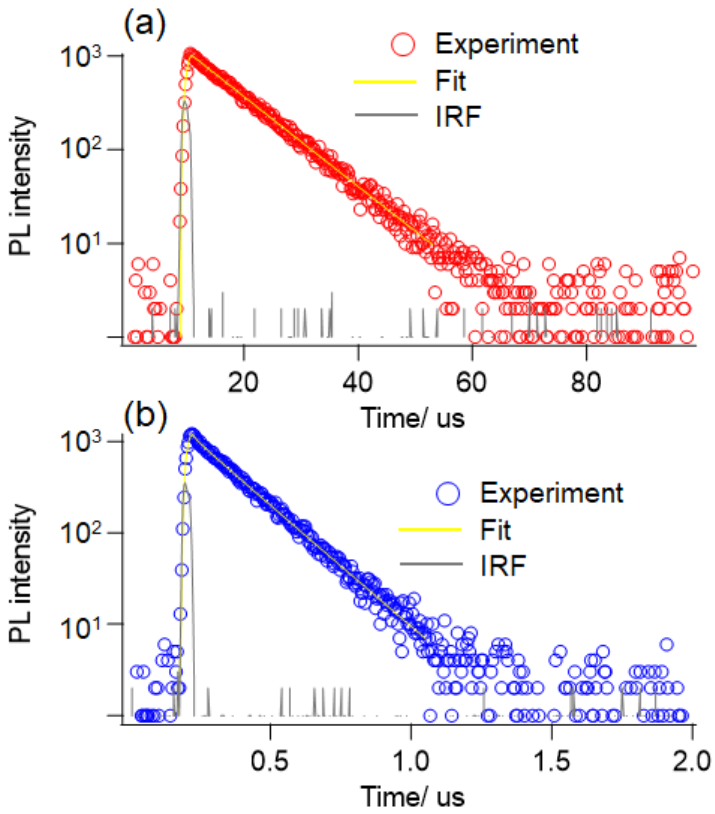

Fig. S4 PL lifetime measurement of $Ag_{29}(BDT)_{12}(TPP)_4$ NCs in pyridine (a) after the photoactivation and (b) after the addition of $TBABH_4$ (ca. 10 equiv. of Ag_{29} NCs). Emission decays were monitored at 700–795 and 600–695 nm for (a) and (b), respectively.

Table S1. Analysis of PL decay curves plotted in Fig. S4

Sample	PL wavelength	Decay times τ_i (α_i, f_i) (μs)	Averaged decay time[a] (μs)	PLQY	k_r (s^{-1})[b]	k_{nr} (s^{-1})[b]
After photoactivation	770 nm	τ = 9.16	-	0.33	3.6×10^4	7.3×10^4
After recovery with $TBABH_4$	675 nm	τ_1 = 0.023 (0.15, 0.024) τ_2 = 0.164 (0.85, 0.976)	$<\tau>$ = 0.161	0.01	6.2×10^{4}[c]	6.1×10^{6}[c]

[a] The averaged decay time is defined by: $<\tau> = \Sigma\alpha_i \times \tau_i^2 / \Sigma\alpha_i \times \tau_i$

[b] k_r = PLQY/τ, k_{nr} = (1–PLQY)×k_r/PLQY

[c] averaged values: $<\tau>$ value was used for the calculation according to [b].

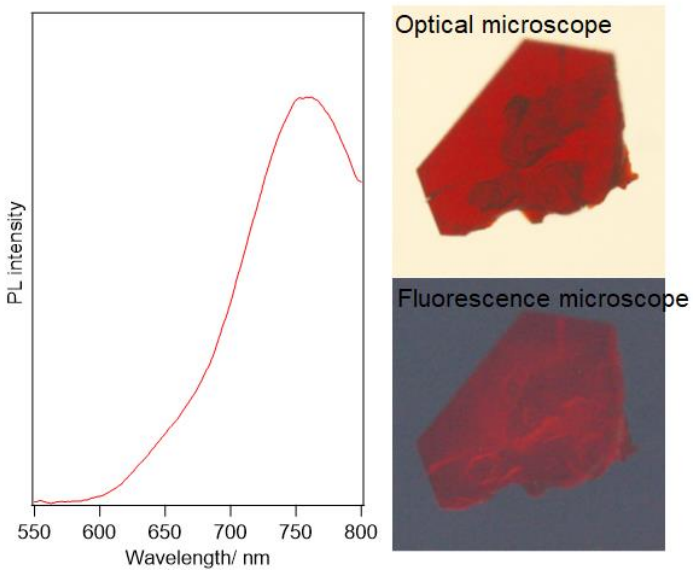

Fig. S5 PL spectrum of a single crystal of the photoactivated Ag_{29} NCs together with microscopic images. Excitation to the crystal was performed with a high-pressure mercury lamp through a band path filer (330–385 nm) and the emission was collected through a long path filter (> 420 nm).

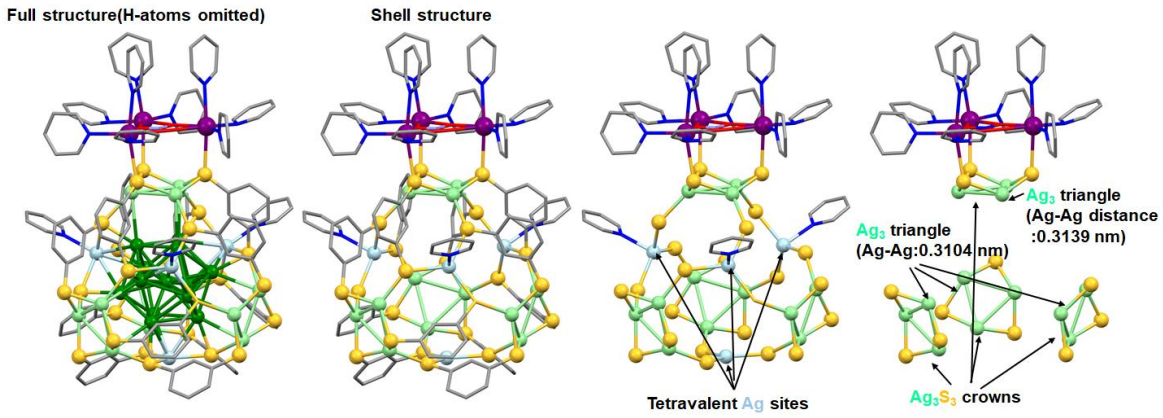

Fig. S6 Detailed X-ray crystal structure of photoactivated Ag_{29} NC.

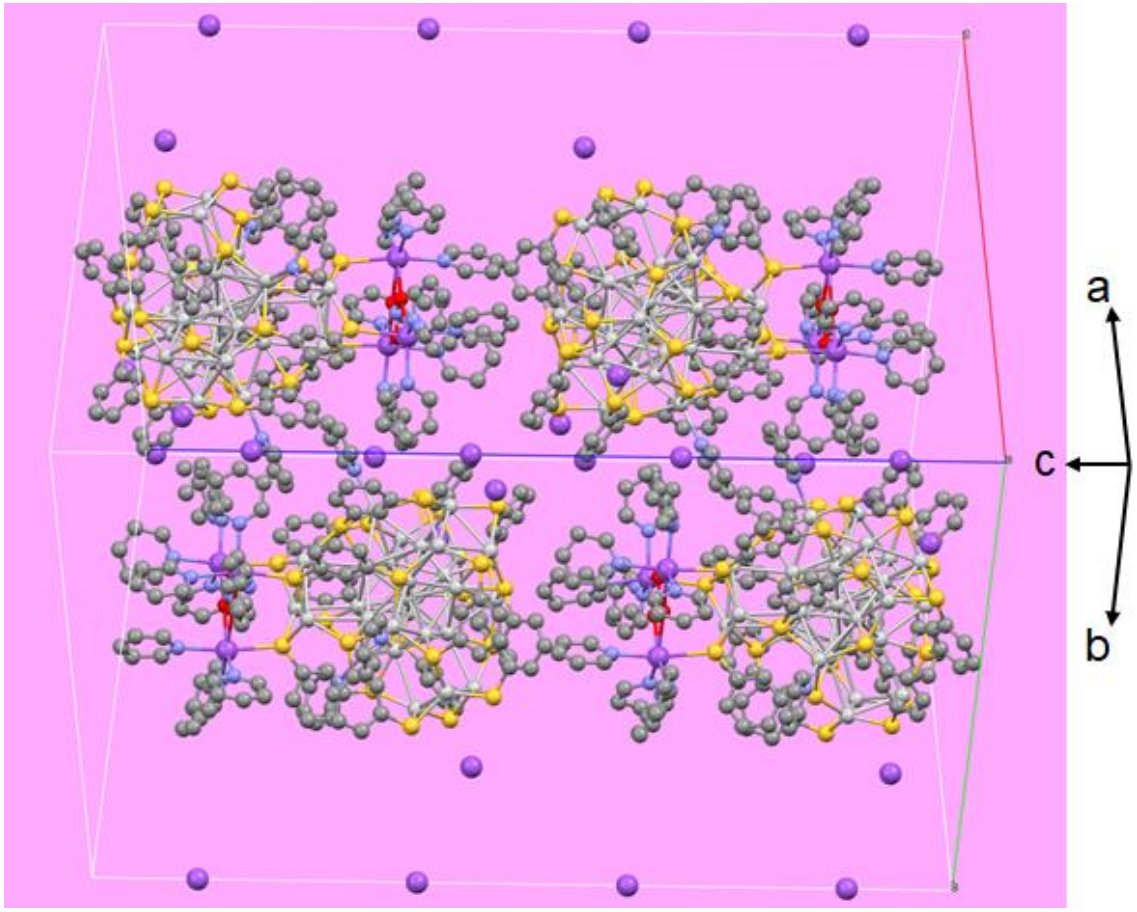

Fig. S7 Packing structure in a unit cell of X-ray crystal structure of photoactivated Ag_{29} NC. Ag, silver; S, yellow; Na, purple, N, blue; O, red; C, grey.

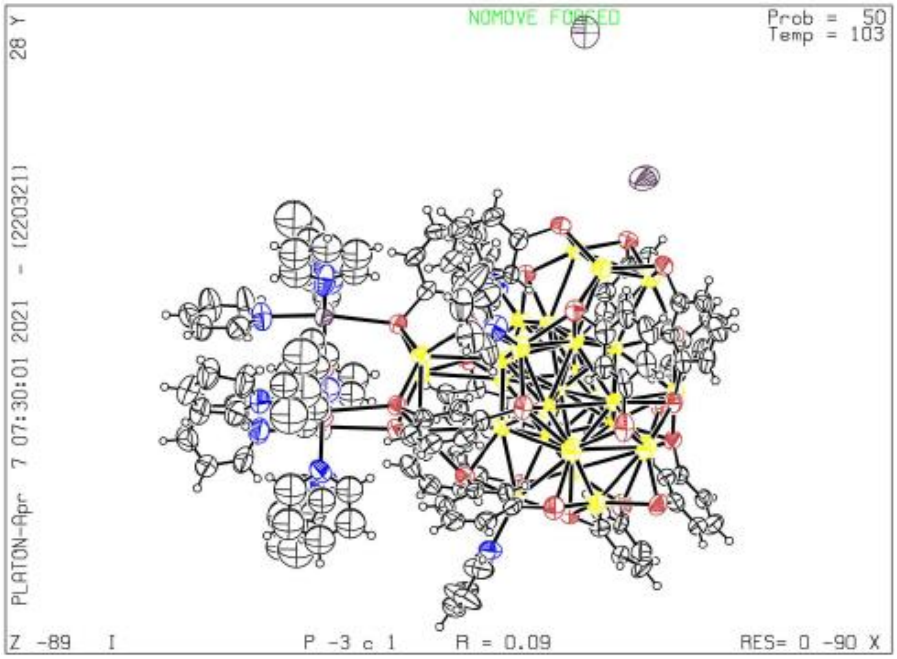

Fig. S8 ORTEP drawing of photoactivated Ag_{29} NC.

Table S2. Crystallographic parameters and refinement details.

formula	C132 H93 Ag 29 N13 Na3 O3 S24 (Na)1
Formula weight	5898.82
Crystal system	Trigonal
Space group	*P*–3c1 (#165)
a (Å)	24.9668(12)
b (Å)	24.9668(12)
c (Å)	44.2740(11)
α (deg)	90
β (deg)	90
γ (deg)	120
V (Å^3)	23900(2)
Z	4
ρ (gcm^{-3})	1.639
μ/ (mm^{-1})	2.564
F(000)	11164
T (K)	103
Crystal size (mm)	0.3 x 0.3 x 0.03
Radiation	MoKα (λ = 0.71075)
Index ranges	-29 ≤ h ≤ 30, -30 ≤ k ≤ 30, -53 ≤ l ≤ 53
Final R indices (I > = 2σ (I))	R_1 = 0.0867, wR_2 = 0.2944
Final R indices (all)	R_1 = 0.1174, wR_2 = 0.3369
CCDC deposition number	2076349

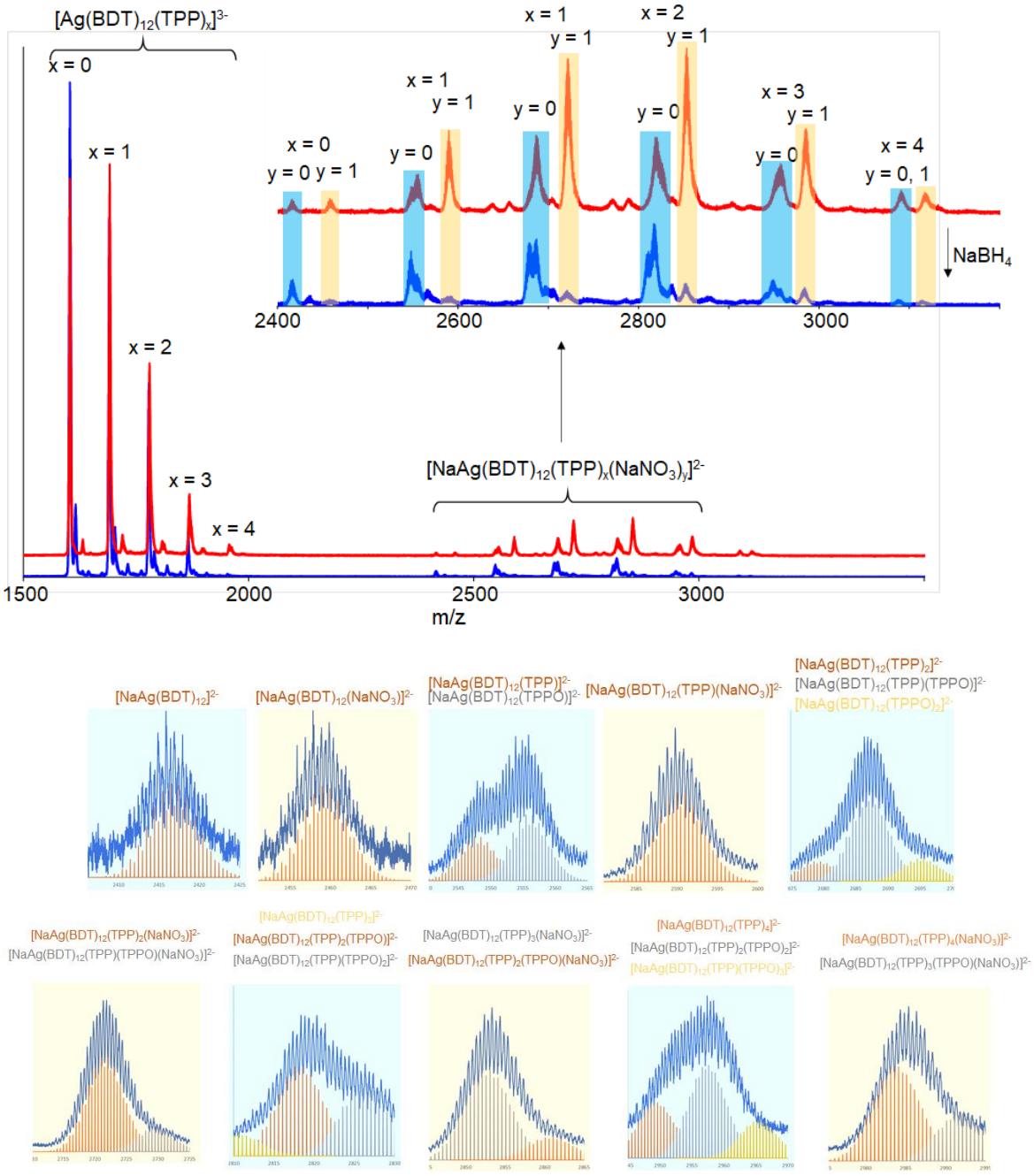

Fig. S9 ESI-MS spectral change of photoactivated Ag_{29} NCs before (red) and after (blue) the addition of $NaBH_4$. Simulated isotope peak patterns are also shown for enlarged peaks.

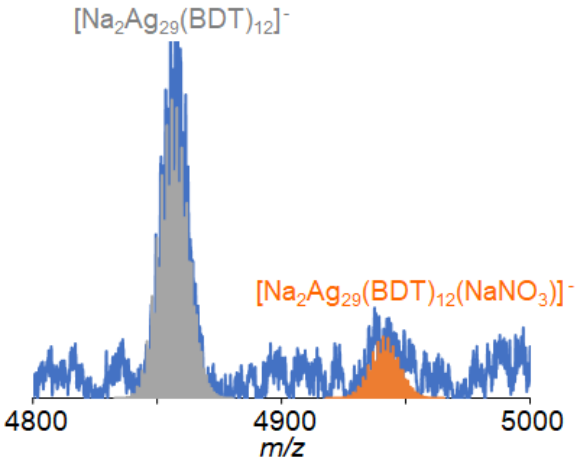

Fig. S10 ESI-MS spectra of photoactivated Ag_{29} NCs in the $z = -1$ region.

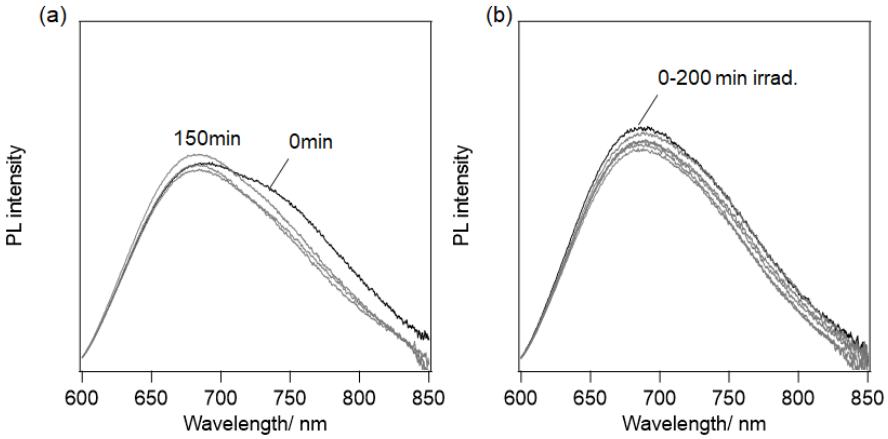

Fig. S11 PL spectral change of Ag_{29} NCs (a) stored in dark and (b) with visible light irradiation (450 nm) under the degassed condition.

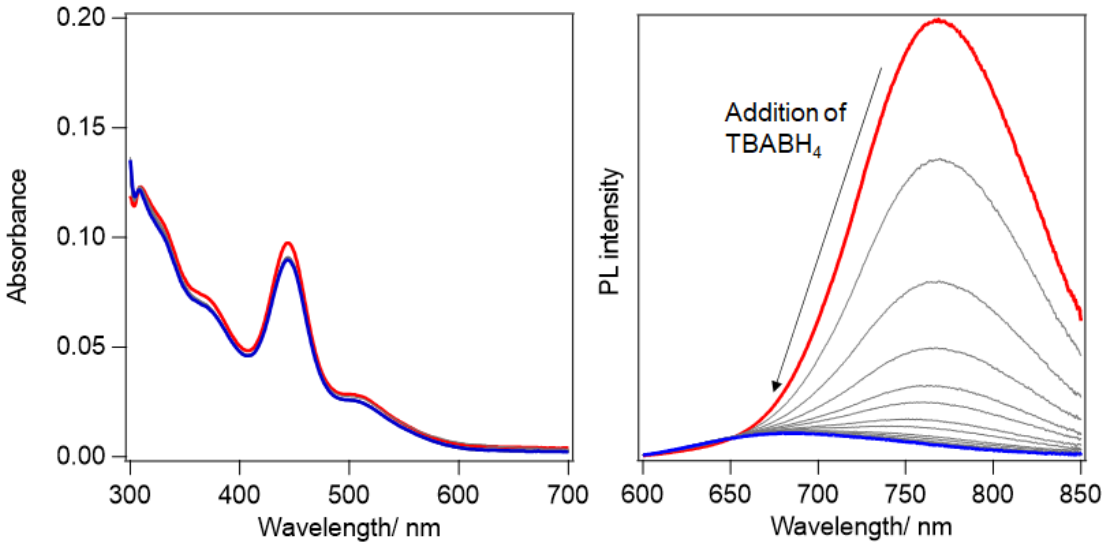

Fig. S12 Absorption and PL spectral change of Ag_{29} NCs in pyridine after the addition of $TBABH_4$ to the photoactivated pyridine solution. Each profile was recorded after every 4 nmol addition of $TBABH_4$. [Ag_{29} NC] = 1.6 μM (3 mL).

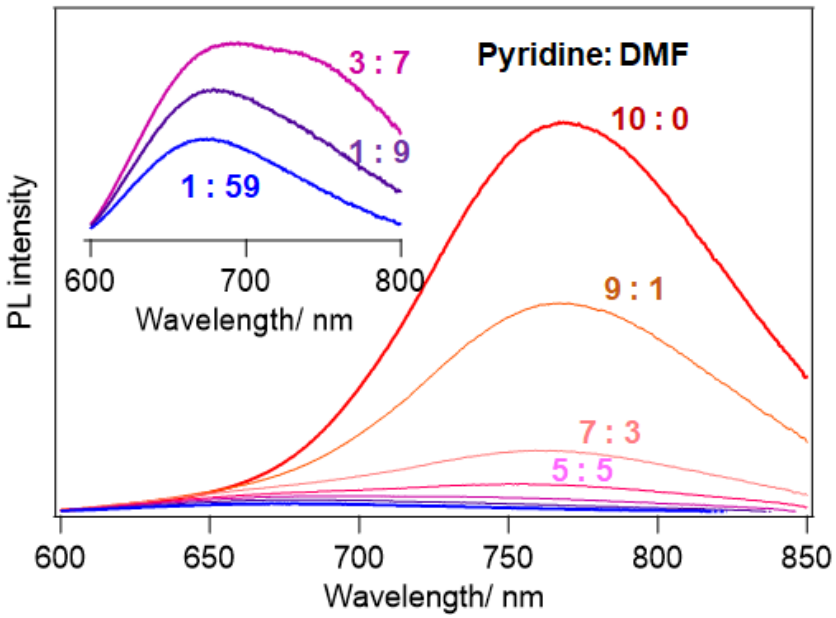

Fig. S13 Solvent-composition dependent PL spectral change of Ag_{29} NCs (λ_{ex} = 450 nm). Inset: Enlarged view for spectra in pyridine/DMF of 3:7, 1:9 and 1:59.

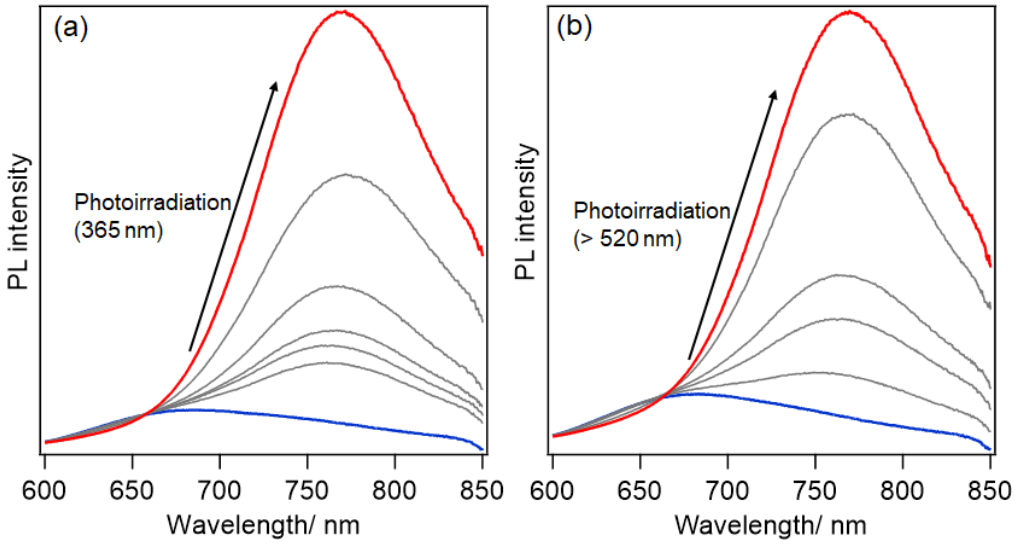

Fig. 14 PL spectral change of Ag29 NCs in pyridine with light irradiation at 365 nm(a) and above 520 nm(b).

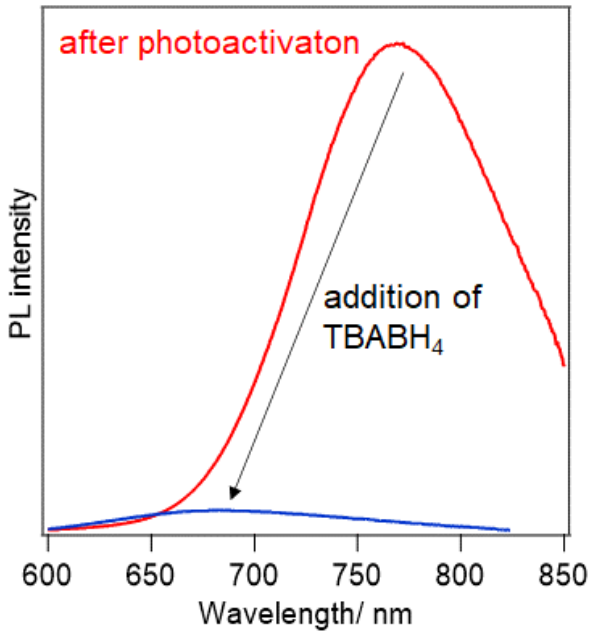

Fig. S15 PL spectral change addition of $TBABH_4$ to the photoactivated Ag_{29} NCs prepared using TBA salt.

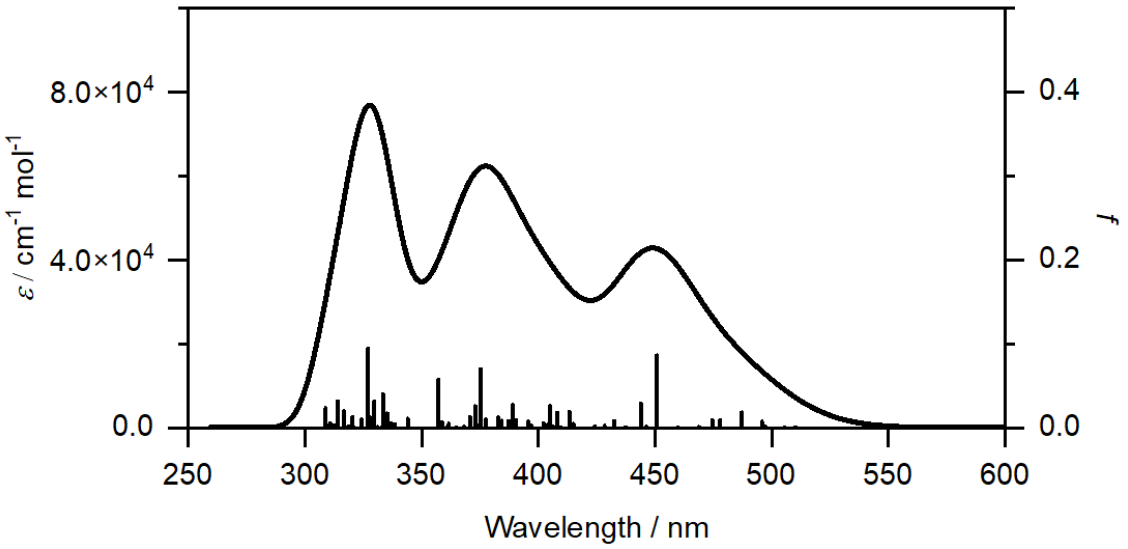

Fig. S16 Theoretical absorption spectrum of $Ag_{29}(BDT)_{12}$ calculated by TD-DFT with B3LYP/LANL2SZ(Ag), 3-21G(S, C, H). The spectrum is convoluted with FWHM of 0.15 eV.

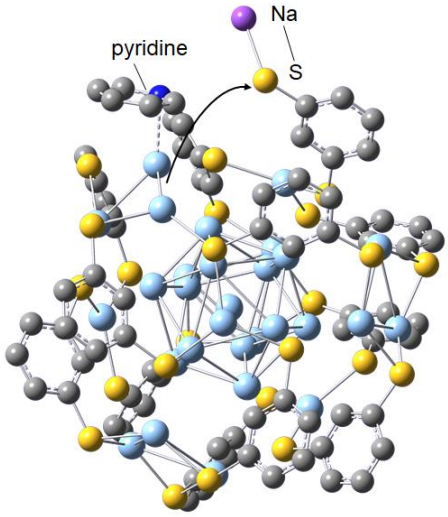

Fig. S17 Optimized structure of $Ag_{29}(BDT)_{11}(BDT\text{-}Na^{+})$(pyridine).

Table S3. Calculated emission energies of $Ag_{29}(BDT)_{12}$ and $Ag_{29}(BDT)_{11}(BDT\text{-}Na^{+})$(pyridine).

		ΔE_{em} (eV)	λ_{em} (eV)
$Ag(BDT)_{12}$	S_1	1.685	736
$Ag(BDT)_{12}$	T_1	1.586	781
$Ag(BDT)_{11}(BDT\text{-}Na^{+})$pry	T_1	1.025	1209

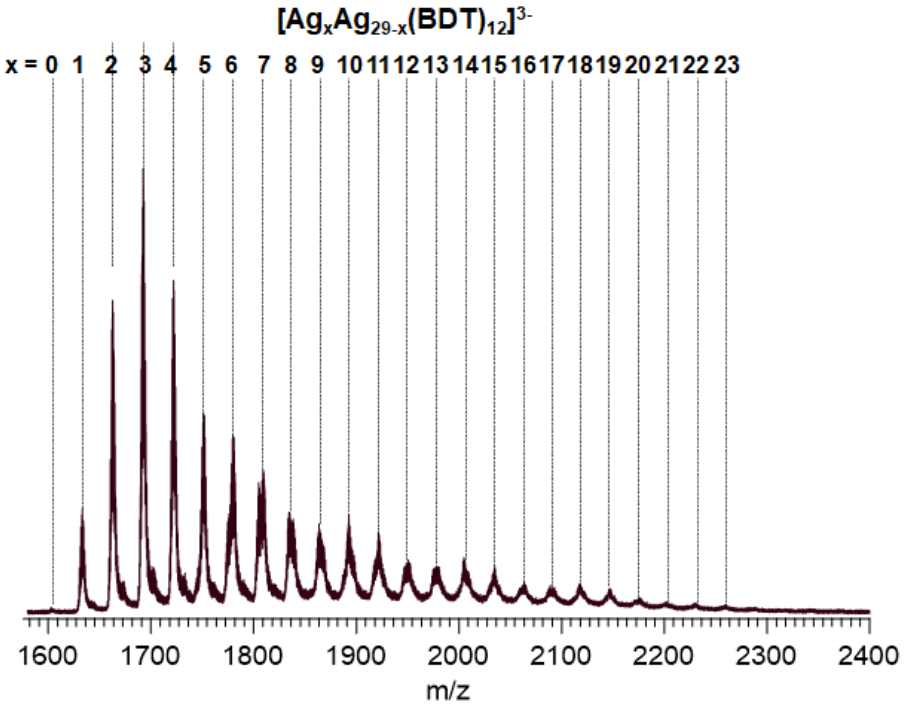

Fig. S18 ESI-MS spectrum of Au-doped Ag_{29} NCs.

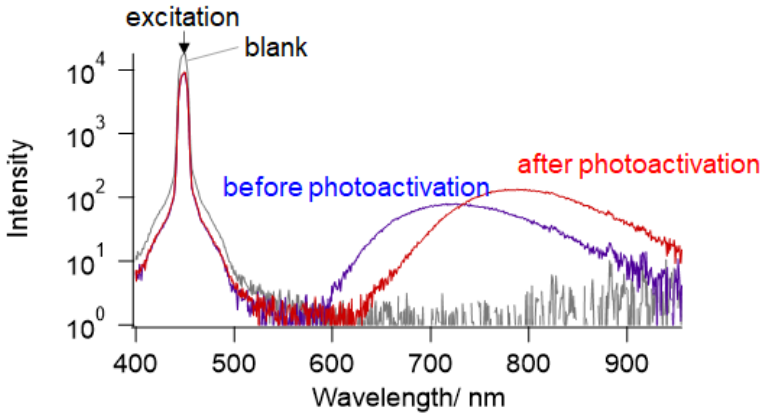

Fig. S19 Determination of absolute PLQY of Au-doped Ag_{29} NCs before and after photoirradiation in pyridine-d_5. The PLQY after the photoactivation was measured to be more than 45% since the upper limit of wavelength range in the PLQY machine is 950 nm.

References

S1 L. G. AbdulHalim, M. S. Bootharaju, Q. Tang, S. Del Gobbo, R. G. AbdulHalim, M. Eddaoudi, D. E. Jiang and O. M. Bakr, *J. Am. Chem. Soc.*, 2015, **137**, 11970-11975.

S2 G. Soldan, M. A. Aljuhani, M. S. Bootharaju, L. G. AbdulHalim, M. R. Parida, A. H. Emwas, O. F. Mohammed and O. M. Bakr, *Angew. Chem. Int. Ed.*, 2016, **55**, 5749-5753.

S3 O. V. Dolomanov, L. J. Bourhis, R. J. Gildea, J. A. K. Howard and H. Pushmann, *J. Appl. Cryst.*, 2009, **42**, 339-341.

S4 G. M. Sheldrick, *Acta Cryst.*, 2015, **A71**, 3-8.

S5 G. M. Sheldrick, *Acta Cryst.*, 2015, **C71**, 3-8.

S6 A. D. Becke, *J. Chem. Phys.*, 1993, **98**, 5648-5652.

S7 P. J. Hay and W. R. Wadt, *J. Chem. Phys.*, 1985, **82**, 270-283.

S8 J. S. Binkley, J.A. Pople and W.J. Hehre, *J. Am. Chem. Soc.*, 1980, **102**, 939-947.

S9 M. J. Frisch, G. W. Trucks, H. B. Schlegel, G. E. Scuseria, M. A. Robb, J. R. Cheeseman, G. Scalmani, V. Barone, G. A. Petersson, H. Nakatsuji et al, Gaussian 16, Wallingford, CT, 2016.